CHAPTER IV
RESULTS AND DISCUSSION

4.1 Characterization of Rice Husk Silica

4.1.1 Chemical Analysis of Silica from Rice Husk

In general, the yield of silica prepared from rice husk was in the range of 15-20% depending on variety, climate, yearly fluctuations and geographic location. From the experiment, the percent yield of silica obtained from rice husk was around 19 % by weight on dry weight basis.

Table 4.1 shows the results obtained from the chemical analysis using X-ray fluorescence (XRF) of ash samples after calcination of rice husk with and without acid leaching pretreatment. The percentages of the metal compounds were calculated with respect to the weight of the sample annealed at around 1 000°C to outgas the adsorbed water vapor.

From the results of X-ray fluorescence analysis, it was found that acid leaching pretreatment by HCl and H_2SO_4 did not give much difference in purity of silicas. It was similar to the study of Leela-Adisorn, (1992) and Yalçin and Sevinç, (2001) concerning preparation and study of silica from rice husk. Furthermore, acid concentration used in this study also did not affect the purity of silica as well. The calcination temperature of 600 and 800°C were chosen to avoid the crystallization of silica which could take place if calcination temperature is above 900°C as reported by Nakata *et al.* (1989). Calcination at 600°C gave a white silica with a lower purity than calcining at 800°C, because it lowered the total organic content (see the value of loss on ignition in Table 1).

Table 4.1 Amounts of silica and other metal compounds in the ash obtained from calcination of rice husk with and without acid pretreatment

Impurities	Sample*								
	A	B	C	D	E	F	G	H	I
SiO_2	97.38	97.59	97.58	97.49	97.33	97.46	98.86	94.61	95.78
TiO_2	<0.05	<0.05	<0.05	<0.05	<0.05	<0.05	<0.05	<0.05	<0.05
Al_2O_3	<0.10	<0.10	<0.10	<0.10	<0.10	<0.10	0.19	0.22	0.85
Fe_2O_3	<0.10	<0.10	<0.10	<0.10	<0.10	<0.10	<0.05	<0.10	0.07
MnO	<0.05	<0.05	<0.05	<0.05	<0.05	<0.05	<0.05	0.10	0.10
MgO	<0.10	<0.10	<0.10	<0.10	<0.10	<0.10	<0.10	0.17	0.24
CaO	<0.10	<0.10	<0.10	<0.10	0.11	<0.10	<0.10	0.50	0.49
Na_2O	<0.10	<0.10	<0.10	<0.10	<0.10	<0.10	<0.10	<0.10	<0.10
K_2O	<0.05	<0.05	<0.05	<0.05	<0.05	<0.05	<0.05	1.73	1.45
P_2O_5	<0.05	<0.05	<0.05	<0.05	<0.05	<0.05	<0.05	0.49	0.48
LOI.**	2.21	2.01	2.01	2.10	2.16	2.14	0.80	1.70	0.33

** LOI. = Loss on ignition.

* A is sample treated with 1 M H_2SO_4 and calcined at 600°C for 6 h,
B is sample treated with 2 M H_2SO_4 and calcined at 600°C for 6 h,
C is sample treated with 1 M HCl and calcined at 600°C for 6 h,
D is sample treated with 2 M HCl and calcined at 600°C for 6 h,
E is sample treated with 0.1 M HCl and calcined at 600°C for 6 h,
F is sample treated with 0.4 M HCl and calcined at 600°C for 6 h,
G is sample treated with 0.4 M HCl and calcined at 800°C for 6 h,
H is untreated sample and calcined at 600°C for 6 h, and
I is untreated sample and calcined at 800°C for 6 h.

4.1.2 Particle Size and Particle Size Distribution

Figures 4.1 and 4.2 illustrate the size distribution curves of the produced silica and commercial silica. The average diameters of silica sample A, B, and C were 20, 24, and 31 μm, respectively. Figure 1, indicates that while the size distributions are broad, most of the silica particles from sample A are finer than those from sample B and C.

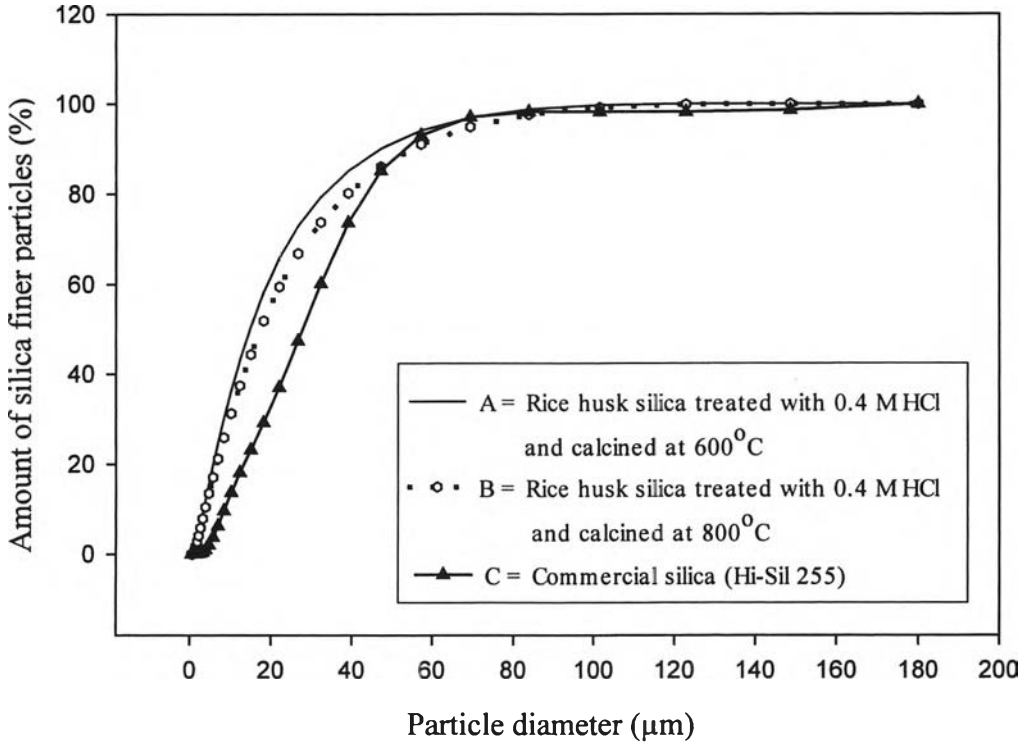

Figure 4.1 The percentage fine and diameter curves of rice husk silica and commercial silica.

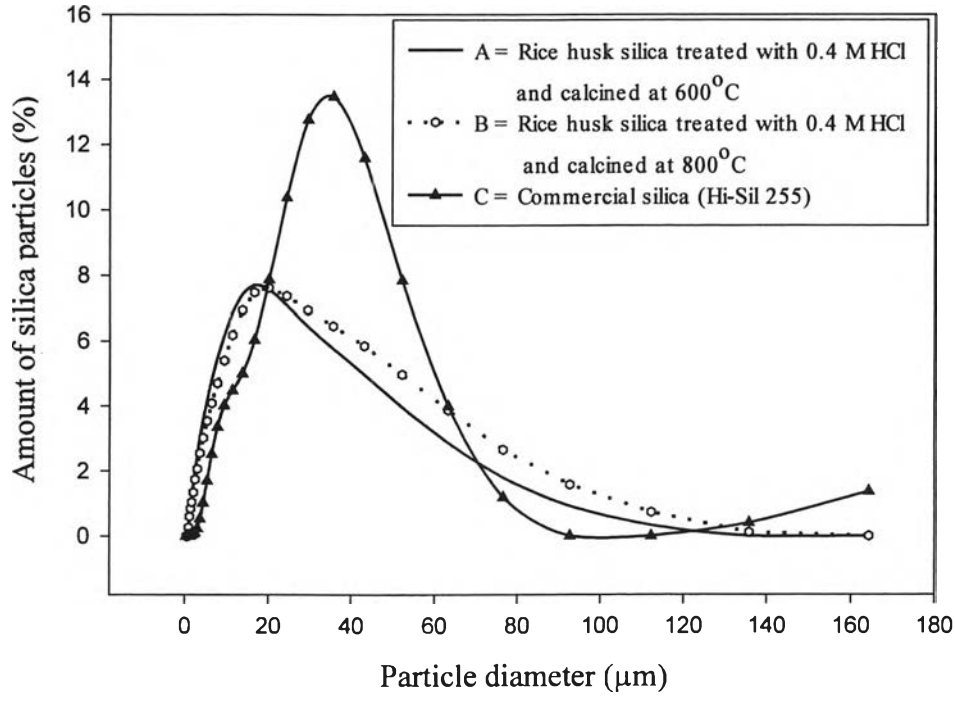

Figure 4.2 Size distribution curves of rice husk silica and commercial silica.

4.1.3 Scanning Electron Micrographs of Rice Husk Silica and Commercial Silica

The scanning electron micrographs of the silica from rice husk and Hi-Sil®255, a commercial porous silica, are shown in Figures 4.3 to 4.7.

Comparison between the rice husk silica and commercial silica images shows that the rice husk silica is flat with irregular shapes while commercial silica is spherical because of the different sources and preparation methods. It is interesting to note that the SEM micrographs show the aggregation and packing of silica prepared from rice husk, not be observed in the commercial silica (see Figures 4.5 and 4.6). It was possible that the aggregation of rice husk silica occurred because its shape was flat and easily piled up.

In addition, the results also show that the morphology of untreated rice husk, acid treated rice husk and rice husk silica (which obtained from calcined at 600 and 800°C) did not change.

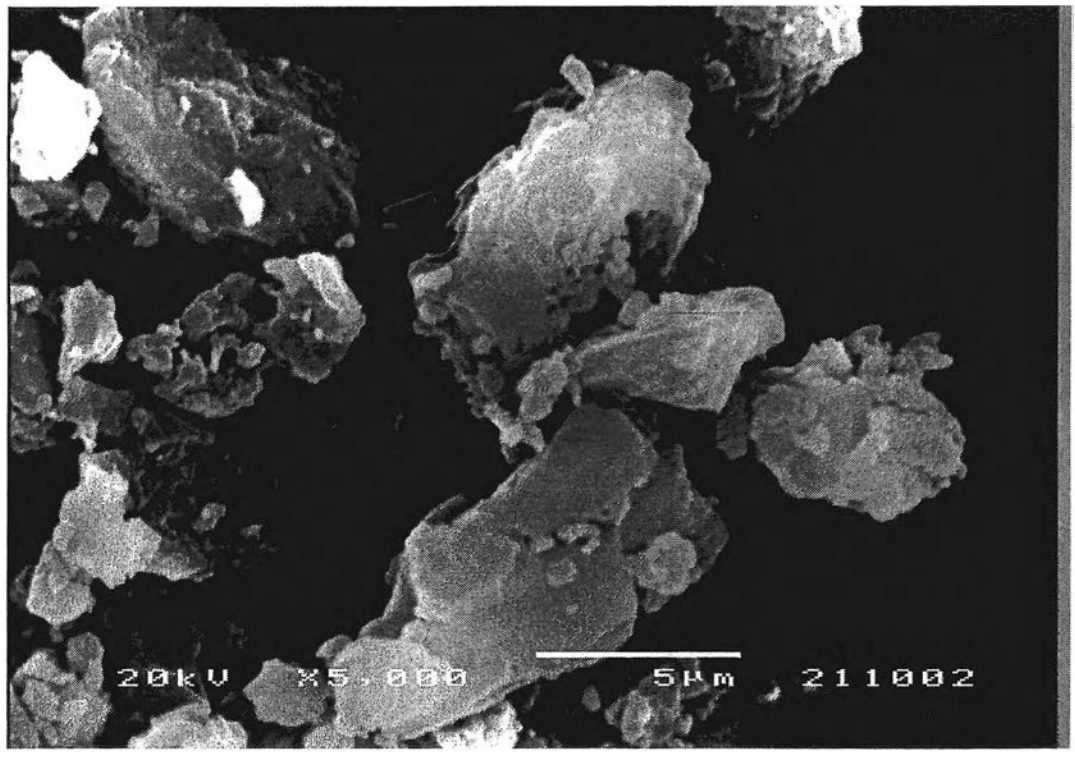

Figure 4.3 SEM micrographs of untreated rice husk with the size of 212 µm.

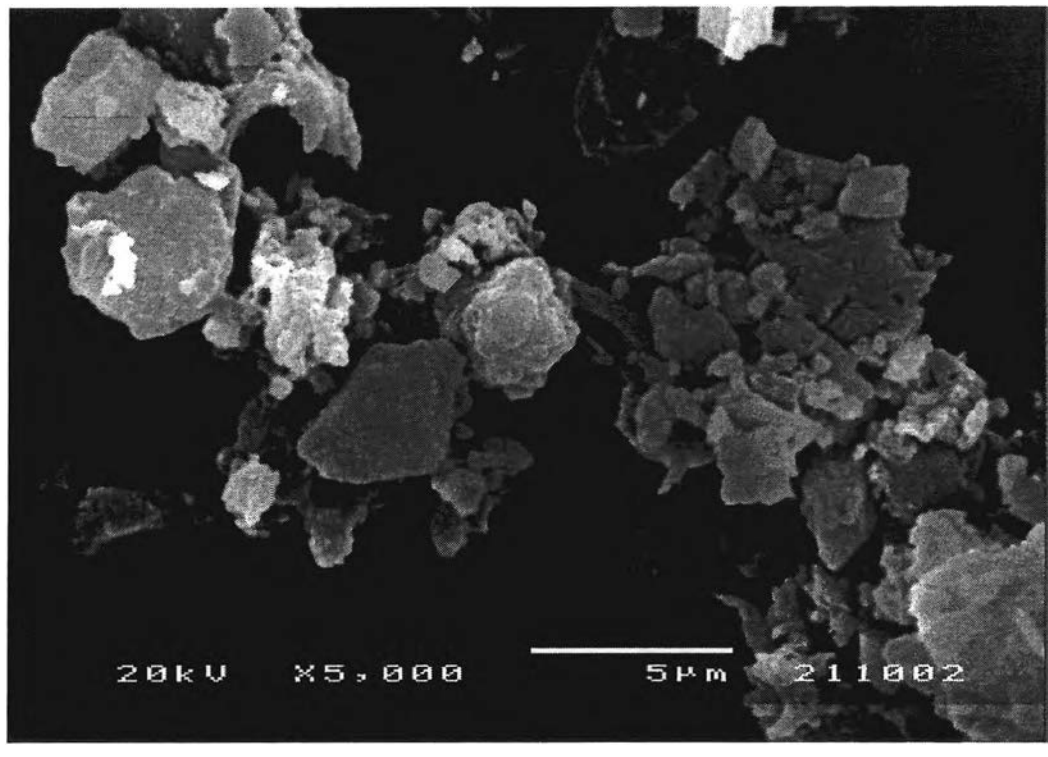

Figure 4.4 SEM micrographs of acid pretreatment with 0.4 M HCl.

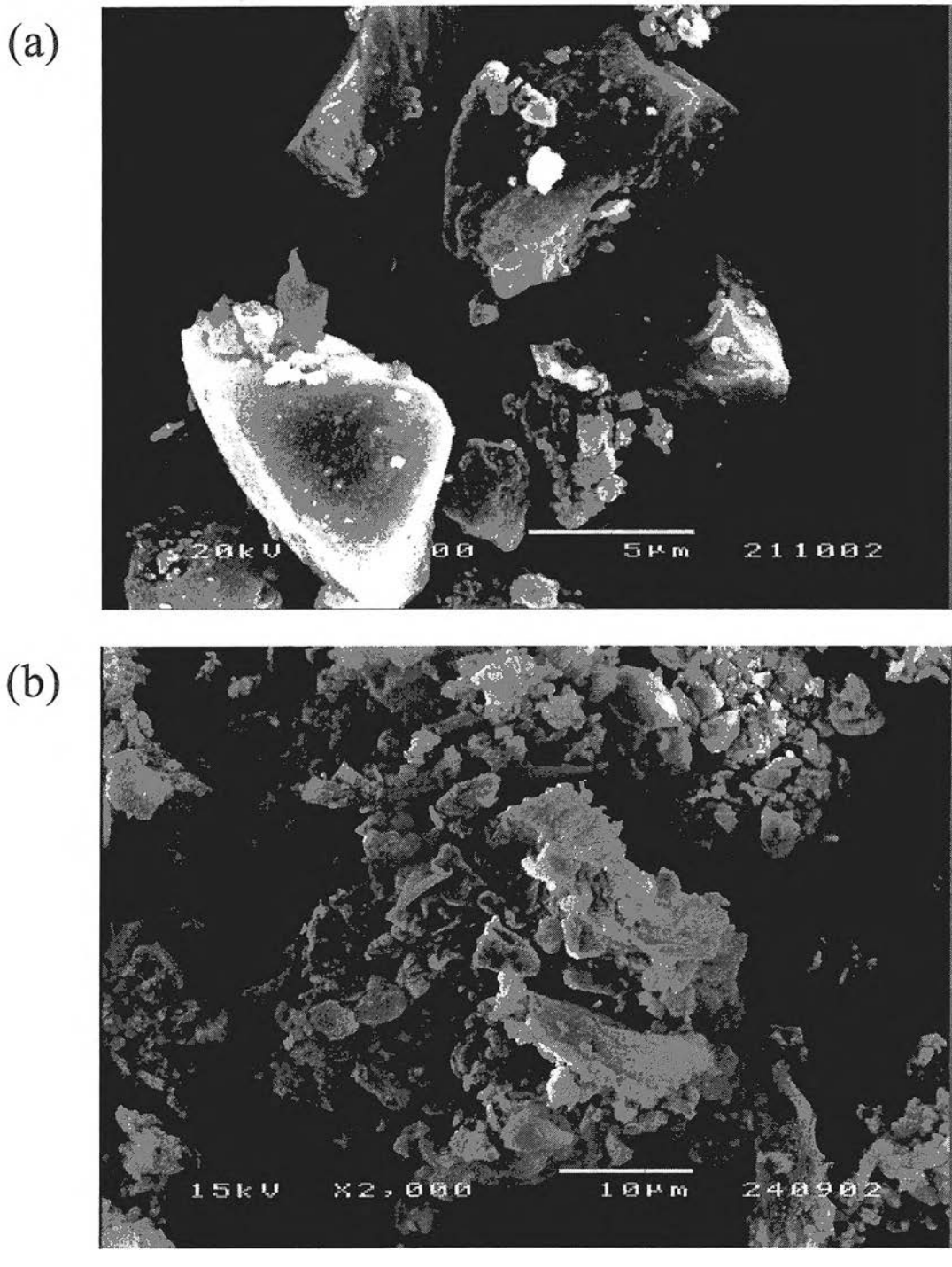

Figure 4.5 SEM micrographs of rice husk silica after calcination at 600°C for 6 h with pretreatment with 0.4 M HCl at a) 5000X magnification, b) 2000X magnification.

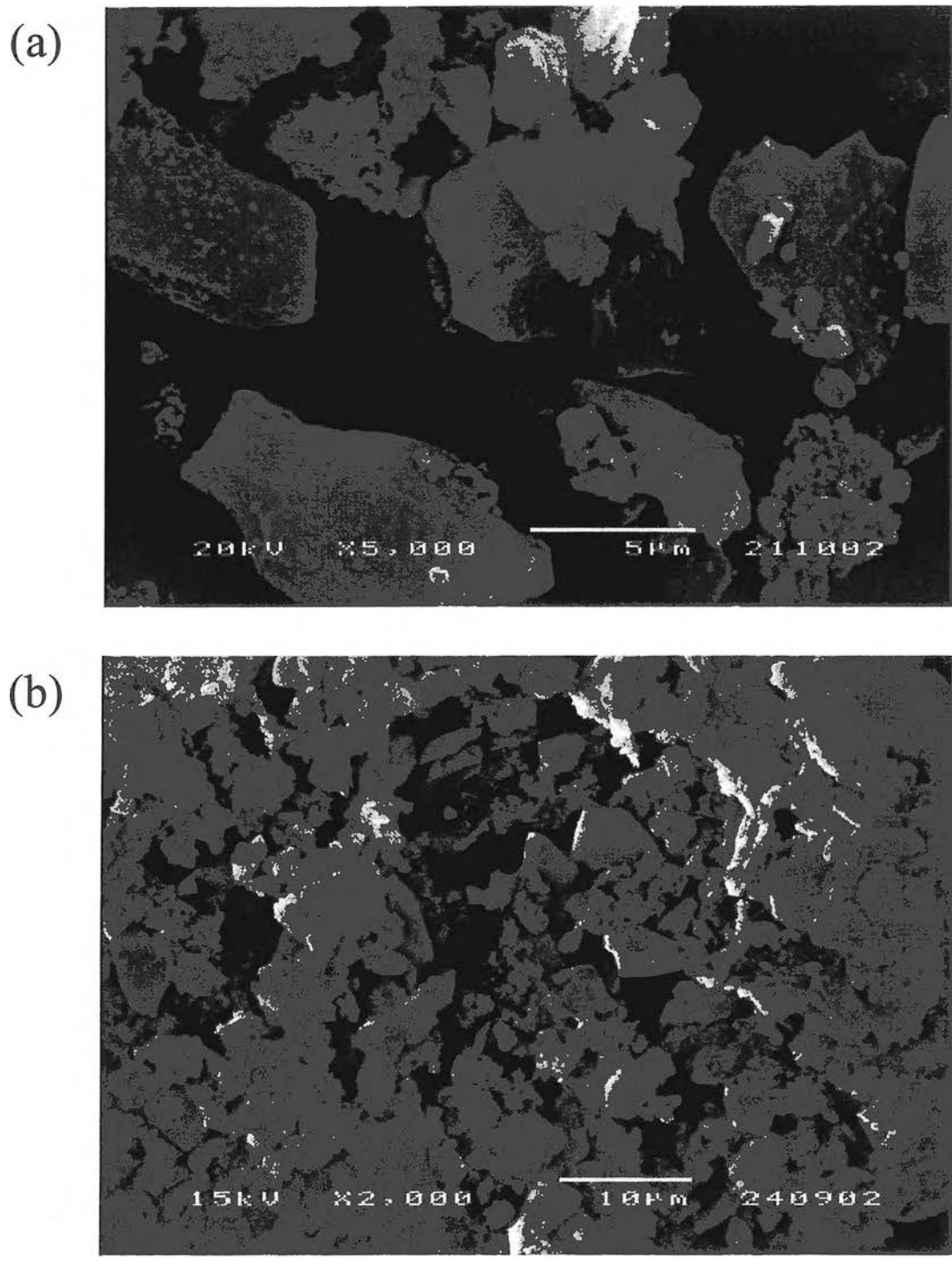

Figure 4.6 SEM micrographs of rice husk silica after calcination at 800°C for 6 h with pretreatment with 0.4 M HCl at a) 5000X magnification, b) 2000X magnification.

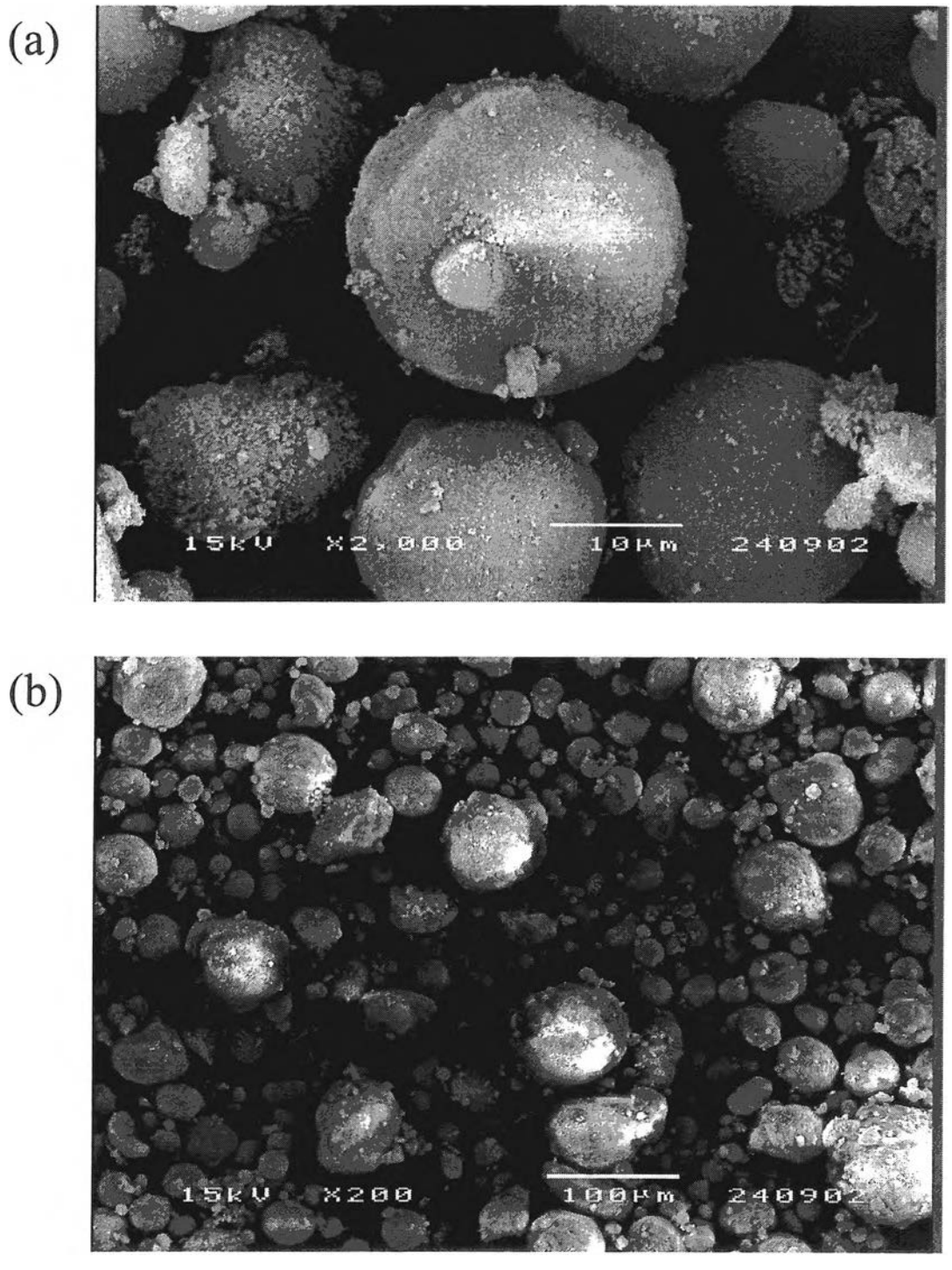

Figure 4.7 SEM micrographs of commercial silica, Hi-Sil®255 at a) 2000X magnification, b) 200X magnification.

4.1.4 X-ray Diffraction Patterns of Rice Husk Silica

The XRDs of silica samples from different preparation procedures are shown in Figure 4.8. The results indicated that rice husk silica and commercial silica samples were amorphous. The amorphous halo is centered on $2\theta = 22°$ and no crystalline structure except for sample of silica which obtained from calcination of rice husk at 800°C without acid leaching pretreatment (sample a) that had a crystalline structure. The XRDs of sample a and c were compared. It was apparent that acid leaching pretreatment affects the crystallization of silica on calcining. These results are similar to those of Real *et al.*, (1996) on preparation of silica from rice husk. One likely explanation is that potassium and other metal compounds contained in rice husk, not removed before calcination, cause the surface melting of SiO_2 particles and accelerate the crystallization of amorphous silica. James and Rao (1986) characterized silica in rice husk ash, produced by isothermal heating of husk at various temperatures. It was found that other metal compounds in rice husk could stabilize and catalyze the formation of cristobalite phase from amorphous silica.

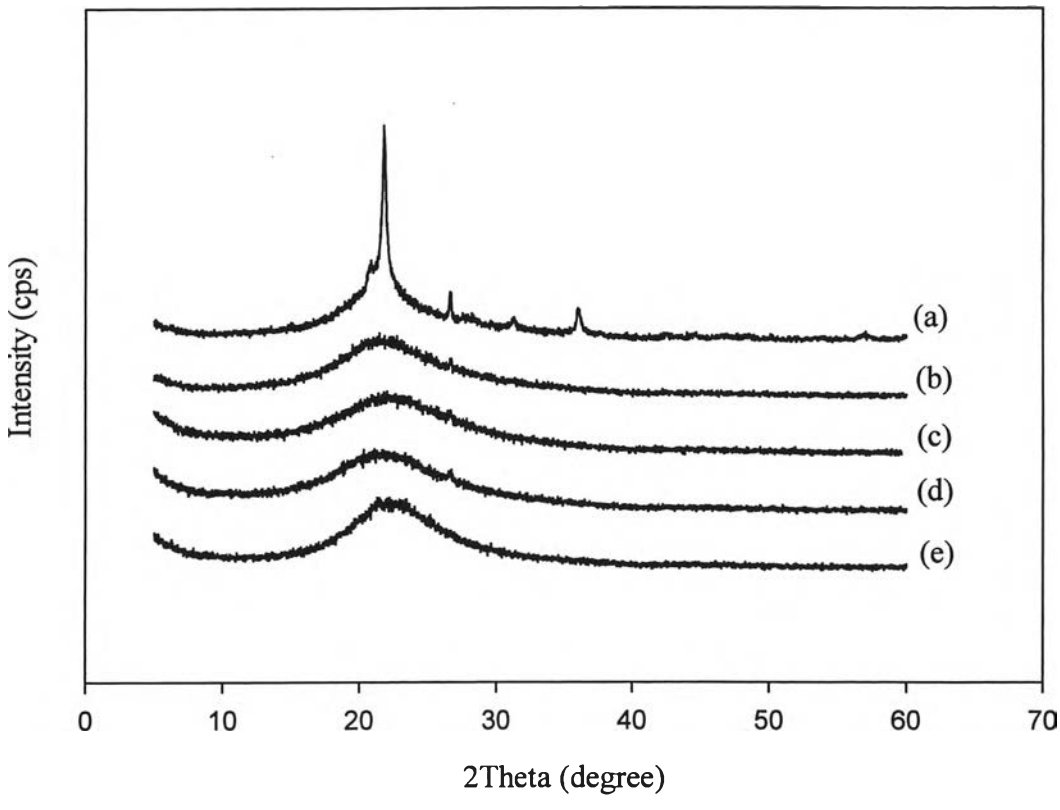

Figure 4.8 XRD powder patterns of silica samples a) rice husk silica after calcination at 800°C for 6 h without pretreatment, b) rice husk silica after calcination at 600°C for 6 h without pretreatment, c) rice husk silica after calcination at 800°C for 6 h with pretreatment with 0.4 M HCl, and d) rice husk silica after calcination at 600°C for 6 h with pretreatment with 0.4 M HCl, and e) commercial silica, Hi-Sil®255.

4.1.5 BET Specific Surface Area, Specific Pore Volume and Specific Pore Diameter of Rice Husk Silica

Specific surface area, which is an important physical property of rice husk silica with and without acid leaching pretreatment and commercial silica were determined. Table 4.2 illustrates the BET specific surface areas, pore volumes and pore sizes of the silica obtained from different preparation procedures. It is evident that all silica samples, which were subjected to acid leaching pretreatment before calcination, had BET specific surface areas higher than that of commercial silica (Hi-Sil® 255). The highest BET specific surface was found to be 349 m^2/g for sample 3

which was treated with 0.4 M HCl for 3 h before calcining at 600°C for 6 h. This value was higher than the values of 182 and 321 m^2/g reported for rice husk silica by Chuayjuljit *et al.*, (2001) and Yalçin and Sevinç, (2001), respectively. On the other hand, silica samples with no acid leaching pretreatment before calcination had lower BET specific surface areas than silica samples with acid leaching pretreatment before calcination. This behavior can be explained that silica with a high specific surface area has a high reaction activity, leading to a strong interaction between the silica and the metallic impurities (especially potassium cations, which is the best promoter for crystallization of tridymite from amorphous silica) contained in the rice husk. This can lead to dramatic decreases in the specific surface area if K^+ cations are not removed prior to the heat treatment (Real *et al.*, 1996).

Table 4.2 BET surface area, pore volume and pore size of unmodified silica

Sample	BET surface area (m^2/g)	Pore Volume (cc/g)	Pore Diameter (A°)
1. Rice husk silica with calcined at 600°C	46.67	0.1941	166.3
2. Rice husk silica with calcined at 800°C	10.77	0.0530	196.7
3. Rice husk silica treated with 0.4 M HCl before calcined at 600°C	349.4	0.4612	52.80
4. Rice husk silica treated with 0.4 M HCl before calcined at 800°C	277.5	0.3563	51.36
5. Silica Hi-Sil®255	184.7	1.514	328.0

The condition for preparation of sample 3 was selected in order to prepare silica with a high purity and high specific surface area from rice husk.

4.2 Modification of Silica Surface via Admicellar Polymerization

4.2.1 Adsorption Isotherm of CTAB on Silica from Rice Husk

The adsorption isotherm of CTAB on silica from rice husk which was pretreated with 0.4 M HCl and then calcined at 600°C for 6 h is shown in Figure 4.9. The CTAB adsorption isotherm illustrates the characteristics regions II, III and IV of the standard adsorption isotherm (Rosen, 1989). From the plateau region data, the maximum adsorption of CTAB on rice husk silica is approximately 64 μmol of CTAB per g of silica. The experimentally determined critical micelle concentration (CMC) of rice husk silica is approximately 1200 μM. Therefore, the initial CTAB concentration giving the equilibrium bulk concentration below CMC for a ratio of 20 g of silica per 250 mL solution is 1250 μM.

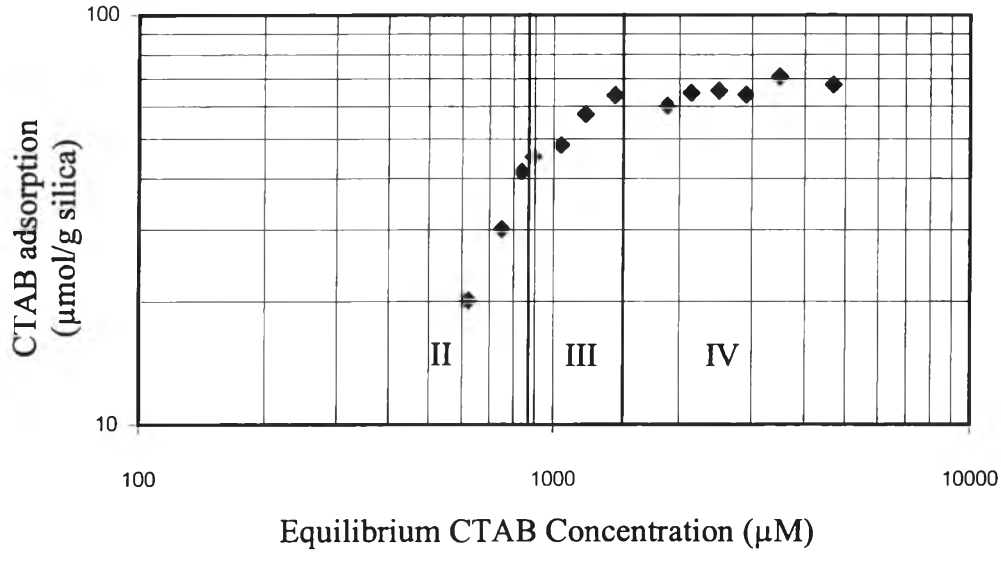

Figure 4.9 CTAB adsorption isotherm on silica from rice husk at pH 8 and 30°C.

The adsorption isotherm of commercial silica (Hi-Sil®255), an amorphous precipitated silica, was measured and a plateau value was found around 580 μmol of CTAB per g of silica (Figure 4.10). This result is consistent with the studies of Kitiyanan *et al.*, (1996) and Chaisirimahamorakot, (2001). The initial

CTAB concentration giving the equilibrium bulk concentration below CMC for a ratio of 20 g of silica per 250 mL is 11,413 μM.

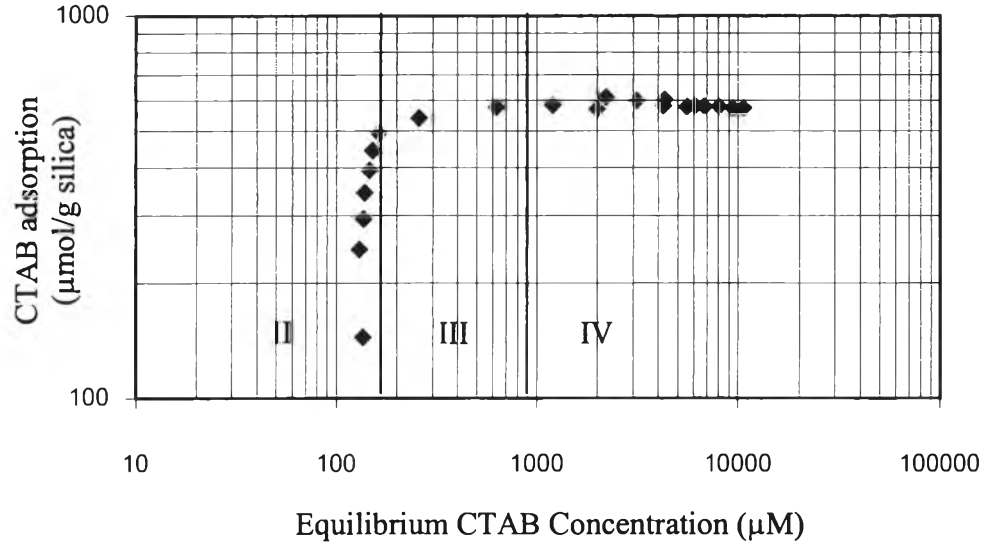

Figure 4.10 CTAB adsorption isotherm on commercial silica (Hi-Sil®255) at pH 8 and 30°C.

It is interesting to note that (comparison between Figures 4.9 and 4.10) commercial silica (Hi-Sil®255) had maximum adsorption of CTAB (580 μmol/g silica) which is much higher than that of the rice husk silica (64 μmol/g silica). In spite of the fact that rice husk silica had BET specific surface area higher than the commercial silica. Results from Table 4.2 suggest that pore diameter of rice husk silica was smaller than that of the commercial silica. The larger pore diameter commercial silica allows CTAB to enter and adsorb on the surface inside the pores but this is not possible for the smaller pore rice husk silica. The areas per molecule of tetradecyltrimethylammonium bromide and octadecyltrimethylammonium bromide were 61 and 64 $Å^2$/molecule, respectively, for area per molecule at surface saturation of surfactants at the water-air interface (Rosen, 1989). Kitiyanan *et al.*, (1996) estimated the area/head group of CTAB to be 62 $Å^2$. Therefore, adsorption of CTAB on rice husk silica occurred only at the outside of the surface of rice husk silica particles while CTAB could enter inside the pore of commercial silica particles.

4.2.2. The Formation of Polystyrene on Modified Silica

The modification of the silica surface was confirmed by FTIR to determine how firmly the polystyrene was attached to the surface of the silica. Figure 4.11 shows FTIR spectra of unmodified rice husk silica, modified rice husk silica, polystyrene standard, and CTAB. No characteristic peaks of polystyrene were observed on the modified rice husk silica (as showed in Figure 4.11(b)). This could be because the high intensity silica adsorption bands interfered with characteristic peaks of polystyrene and the amount of polystyrene coated on rice husk silica was very low when compared to the amount of silica. Figure 12 illustrates the FTIR spectra of unmodified Hi-Sil®255, modified Hi-Sil®255, polystyrene standard, and CTAB. The result was similar to that of rice husk silica. The spectrum of the modified Hi-Sil®255 (see in Figure 4.12(b)) shows small absorbent peaks of methylene C-H stretching in the range of 2980-2840 cm^{-1}, suggesting the presence of CTAB and polystyrene on silica. Therefore, in order to confirm the polymerization of styrene on the surface of silica, polystyrene on the modified silicas was later extracted with THF via the polymer extraction process.

The extracted polymers from both rice husk silica and Hi-Sil®255 were characterized by FTIR technique and compared with to the spectrum of a polystyrene standard in order to confirm that polystyrene was formed on the silica surface (as shown in Figures 4.13 and 4.14, respectively). All peaks observed in the spectra of extracted polymer from modified silica were consistent with the polystyrene standard. It clearly showed important peaks that represented the characteristic of aromatic C-H stretching at the wavenumber of 3100-3000 cm^{-1}, aromatic C ⋯ C at 1600 cm^{-1}, aromatic C=C continued at 1494 cm^{-1} and 1455 cm^{-1}, and mono-substituted benzene ring at 751 cm^{-1} and 701 cm^{-1}. This result confirmed that polystyrene was formed on the surface of modified silica particles by admicellar polymerization.

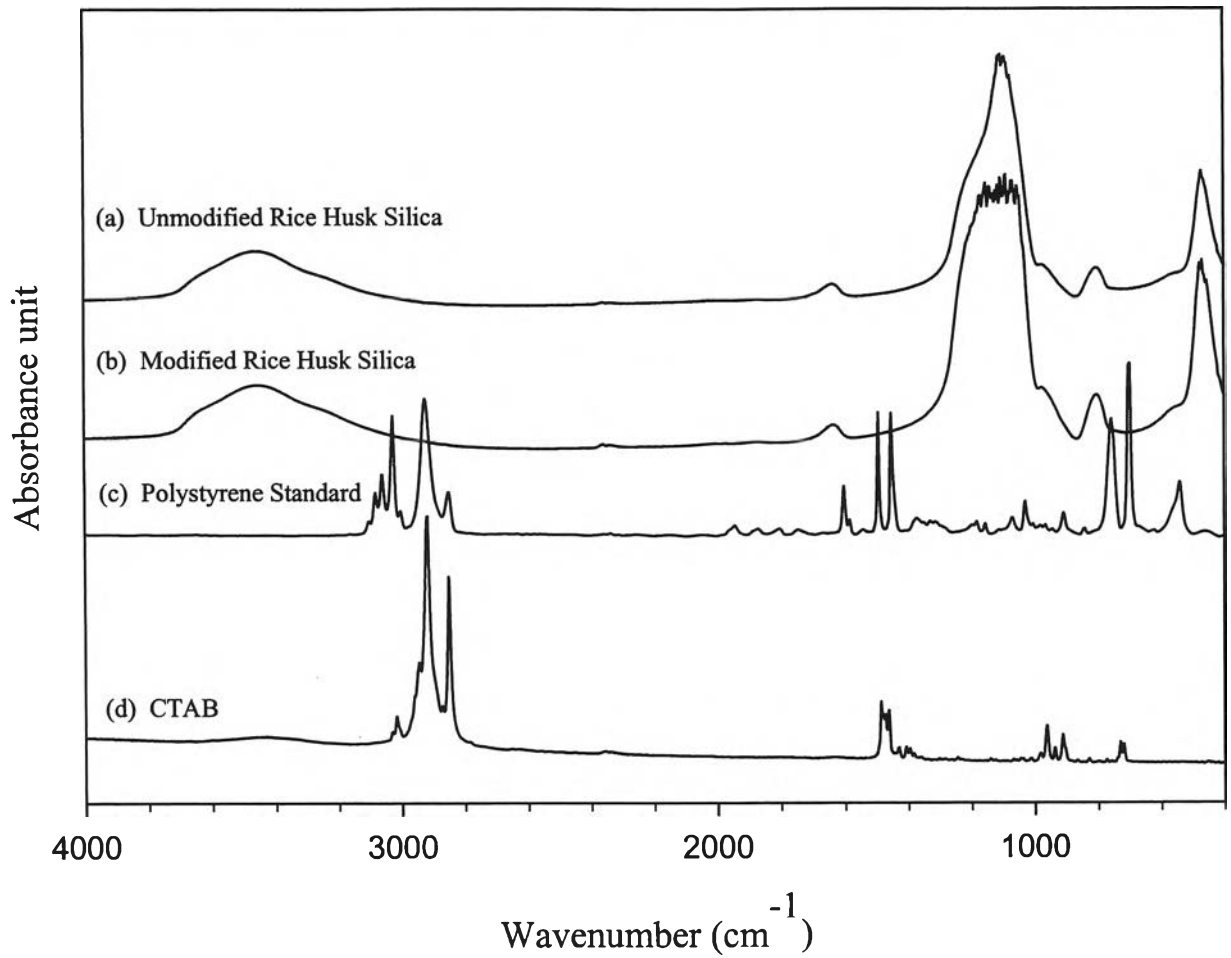

Figure 4.11 FTIR spectra of (a) unmodified rice husk silica, (b) modified rice husk silica, (c) polystyrene standard, and (d) CTAB.

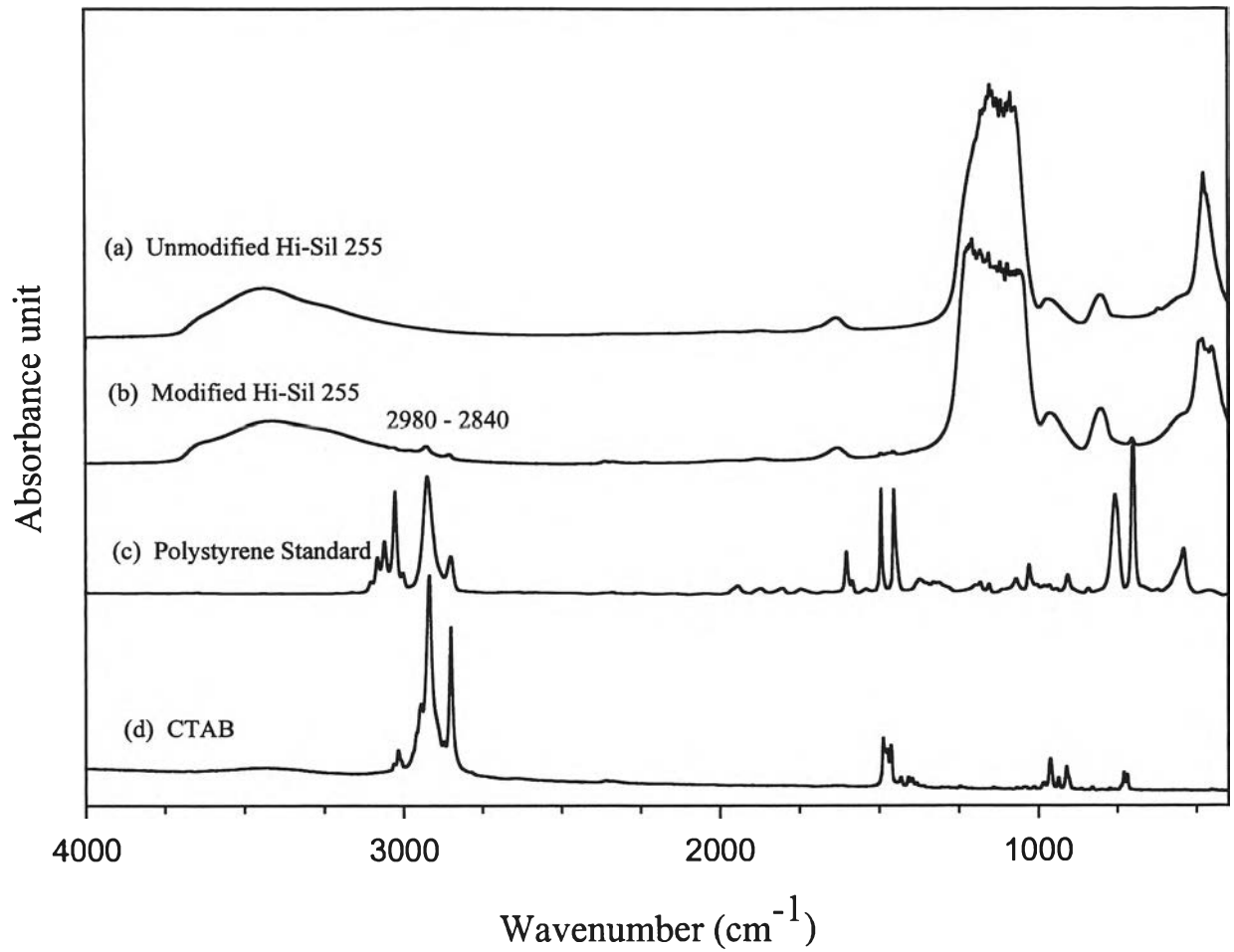

Figure 4.12 FTIR spectra of (a) unmodified Hi-Sil®255, (b) modified Hi-Sil®255, (c) polystyrene standard, and (d) CTAB.

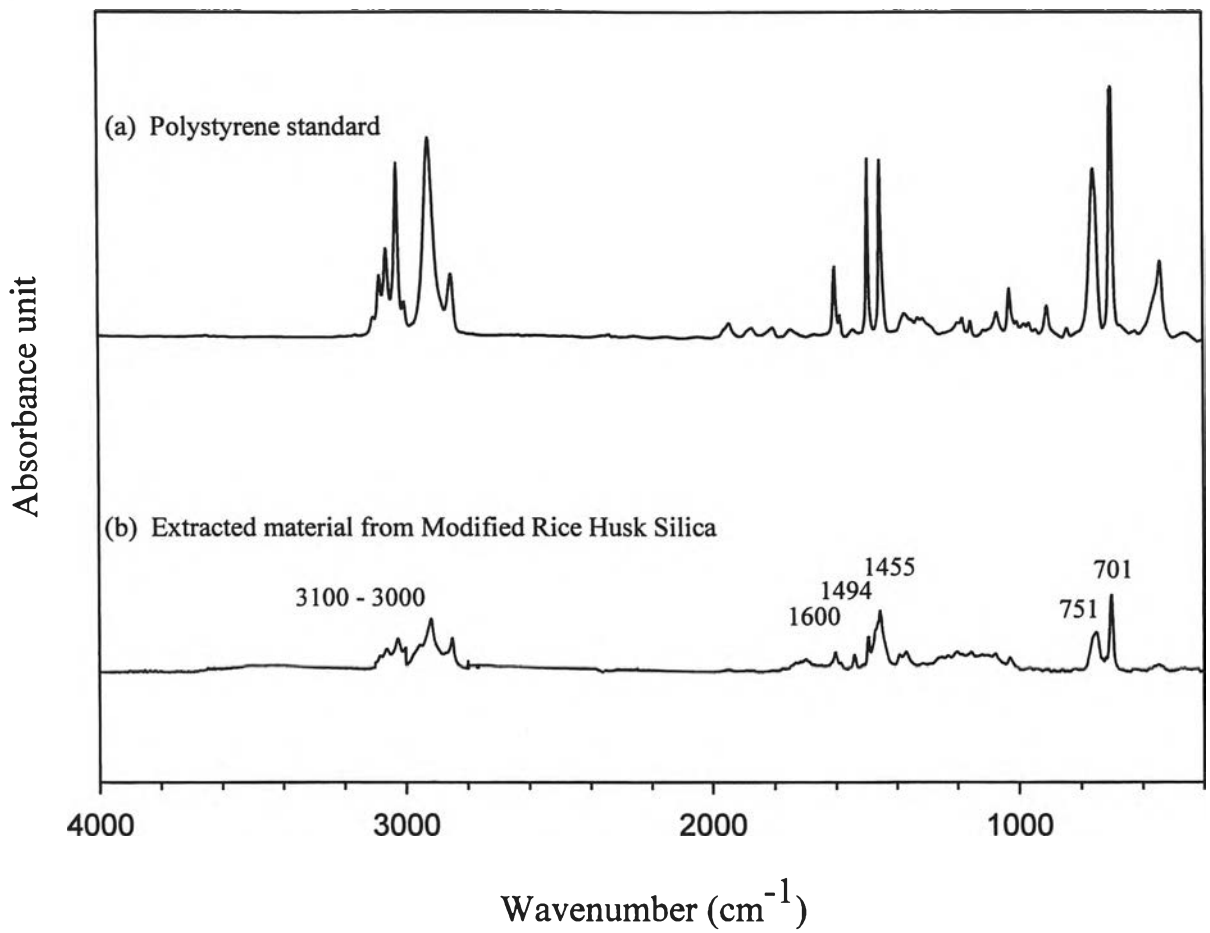

Figure 4.13 FTIR spectra of (a) polystyrene standard and (b) extracted material from modified rice husk silica.

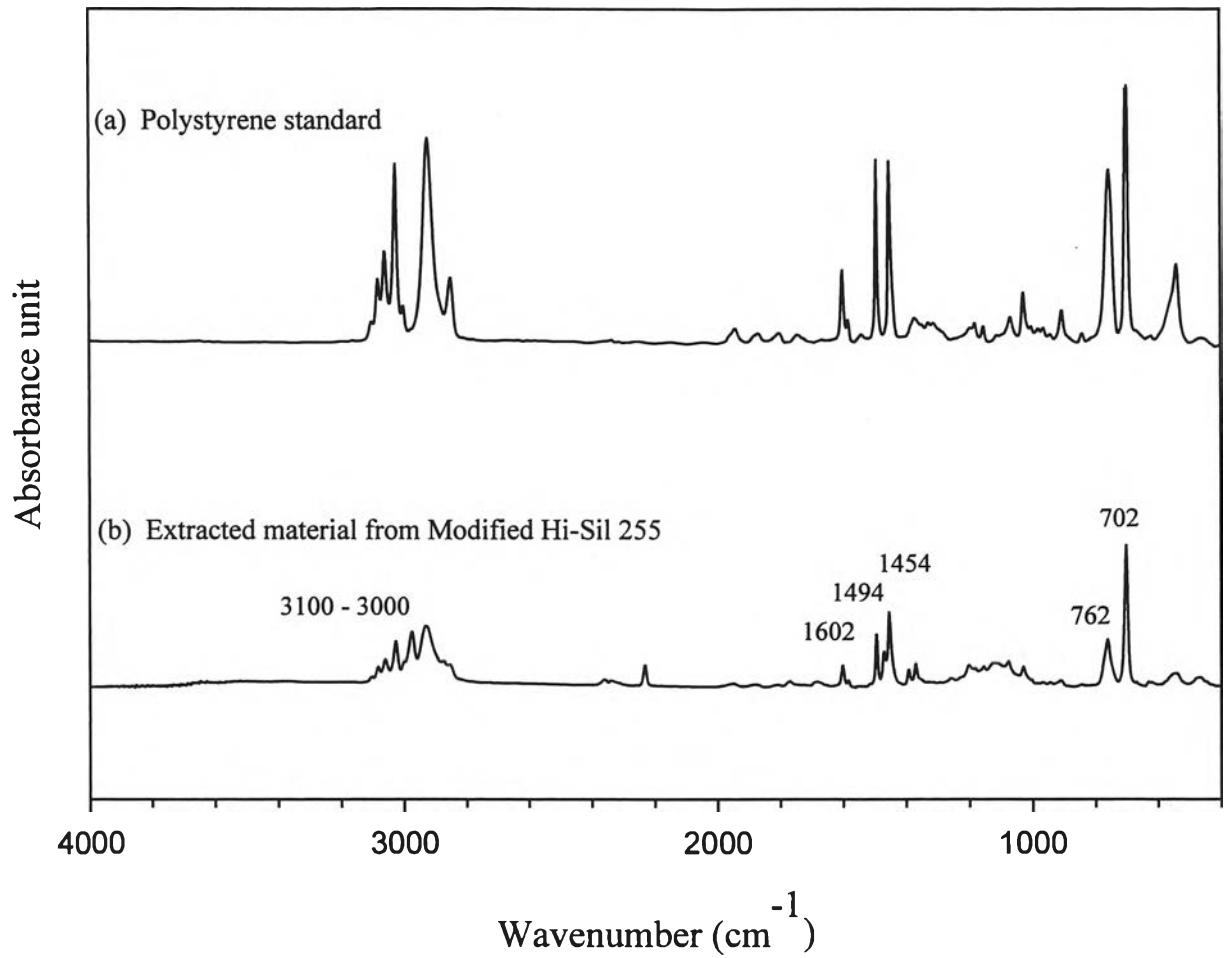

Figure 4.14 FTIR spectra of (a) polystyrene standard and (b) extracted material from Hi-Sil®255.

4.2.3 Thermogravimetric Analysis

The modified silica samples were examined by thermogravimetric analysis (TGA) to study thermal stability of the extracted polystyrene and to verify the existence of polystyrene formed on the silica.

The TGA of the unmodified silica (see Figure 4.15) shows a loss of water from the unmodified rice husk silica and Hi-Sil®255 below 150°C. So, any mass changes above 150°C should be the result of the surface modification. Figure 4.16 shows the decomposition of polystyrene (STYRON™ 656D) in the range of 350°-450°C. Figure 4.17 shows the decomposition of CTAB between 200°-300°C. Figure 4.18 shows the decomposition of CTAB adsorbed onto the rice husk silica and Hi-Sil®255 which appeared to occur in two steps. The first step was from 170° to 310°C and the second step was from 310° to 450°C. The second peak of the weight loss might be a result from the stronger bonding, chemisorption, between CTAB and silica (Nontasorn, 2002).

The decompositions of polystyrene on the modified surfaces of rice husk silica and Hi-Sil®255 from admicellar polymerization are shown in Figure 4.19. The TGAs of both modified silicas clearly show decomposition of the components on the surface of silica, which degraded at the temperature between 170°-320°C, were mainly of CTAB. The second weight loss between 320°-450°C was due to the decomposition of CTAB chemisorped on the silica as well as polystyrene decomposition at 350°-450°C. This decomposition was confirmed by thermogram of the extracted polystyrene in Figure 4.20.

Figure 4.20 shows the TGA of the extracted polystyrene from both modified rice husk silica and Hi-Sil®255. The TGAs of both extracted polystyrene clearly show that decomposition temperature of extracted polystyrene occurred in two steps between 170°-350°C and 350°-450°C. From the TGA of the extracted polystyrene, the result suggested that the degradation below 350°C was caused by degradation of CTAB trapped in the extracted polystyrene and above 350°C was caused by degradation of polystyrene as well as CTAB chemisorped on the silica.

Figure 4.21 shows TGAs of modified rice husk silica and Hi-Sil®255 after extraction. Comparisons of the modified silica before and after extraction

(Figures 4.19 and 4.21), the percentage mass loss and derivative mass from thermograms of both modified silicas after extraction were lower than those obtained before extraction. Thus, most of polystyrene is removed from silica particles after extraction.

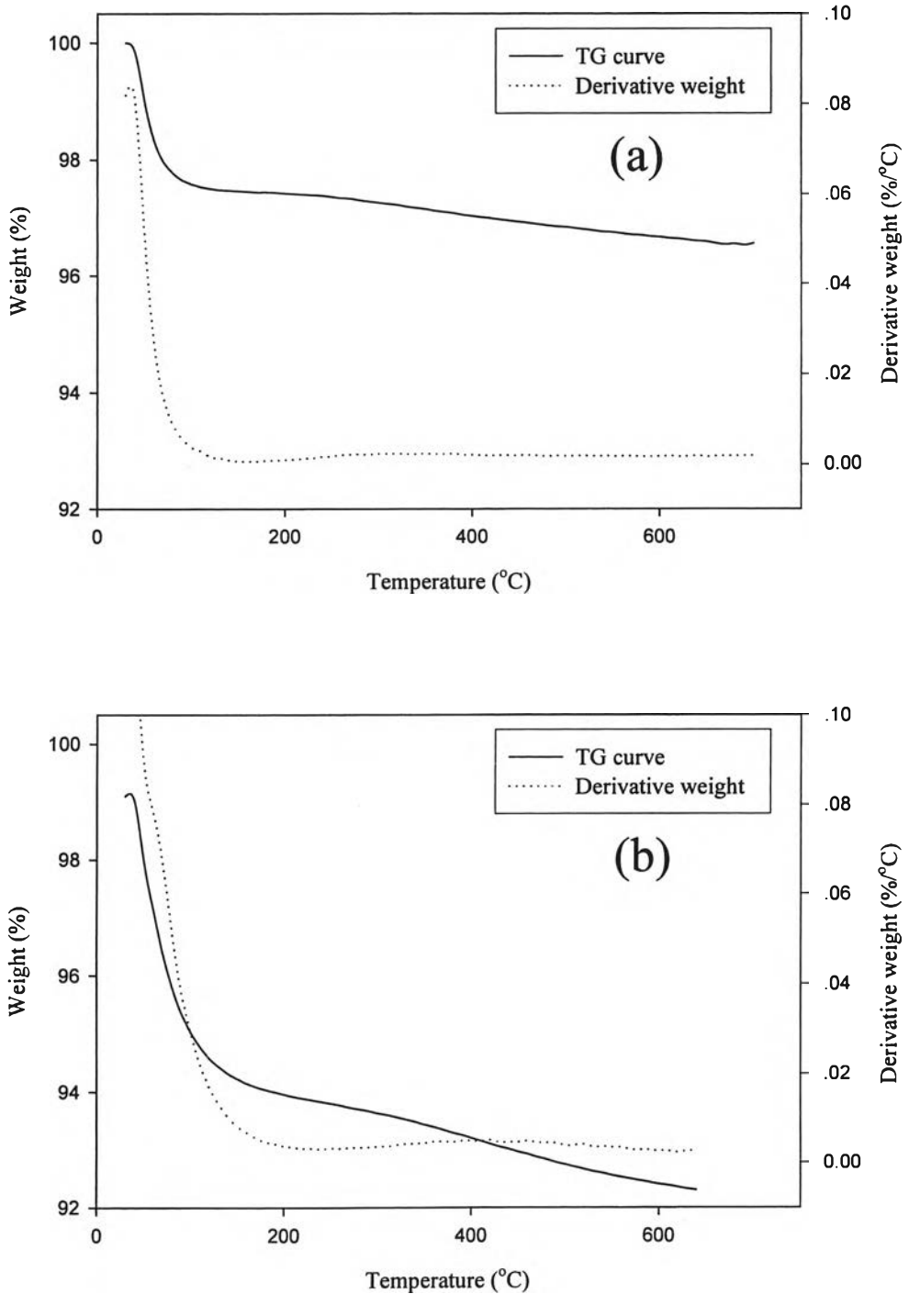

Figure 4.15 TGA traces of unmodified silica a) Rice husk silica, and b) Hi-Sil®255.

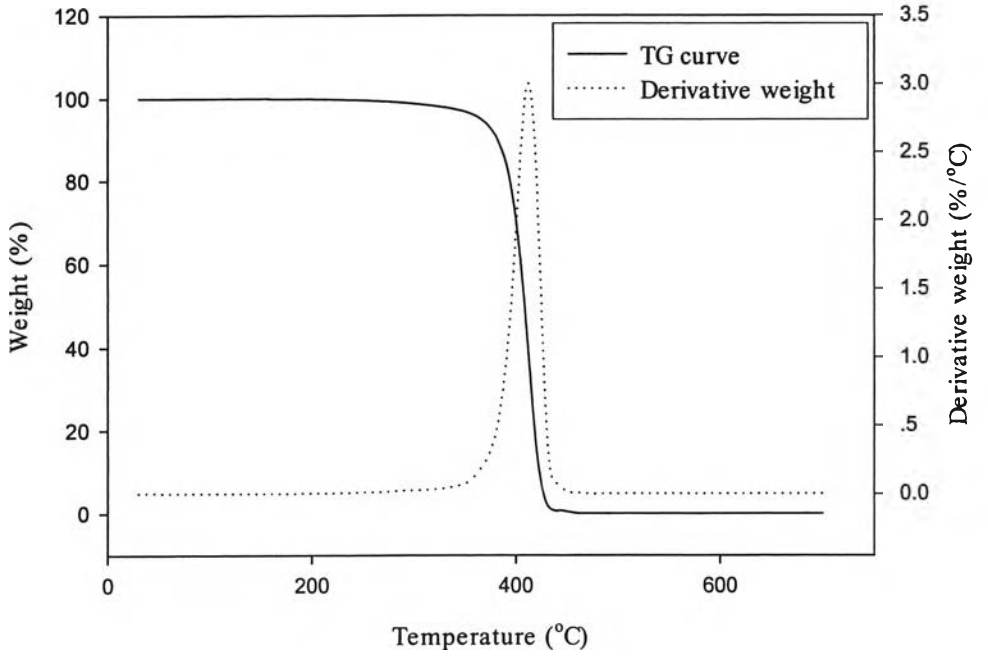

Figure 4.16 TGA trace of polystyrene (STYRON™ 656D).

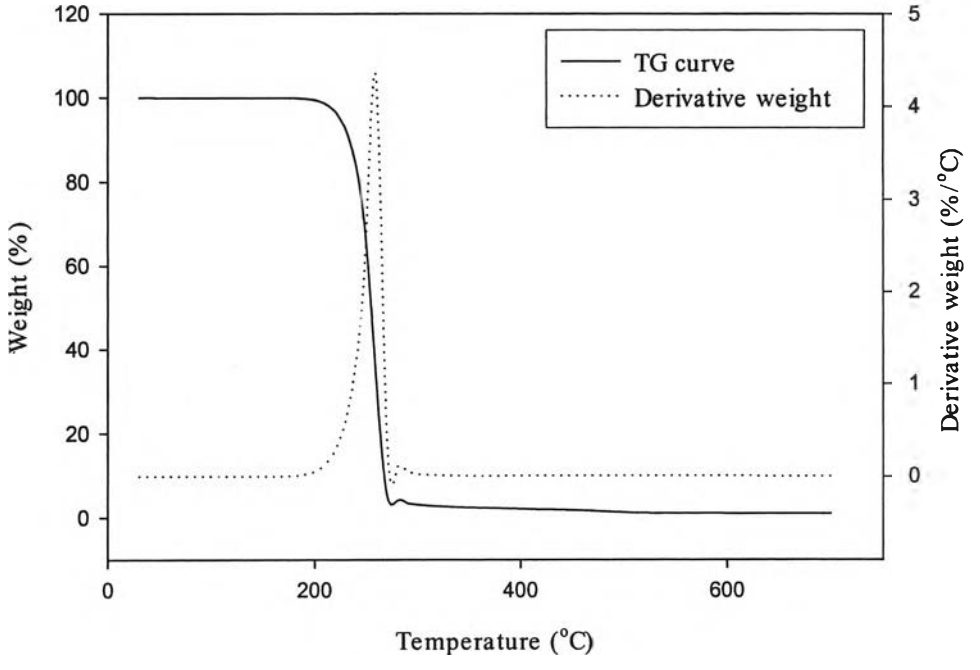

Figure 4.17 TGA trace of CTAB.

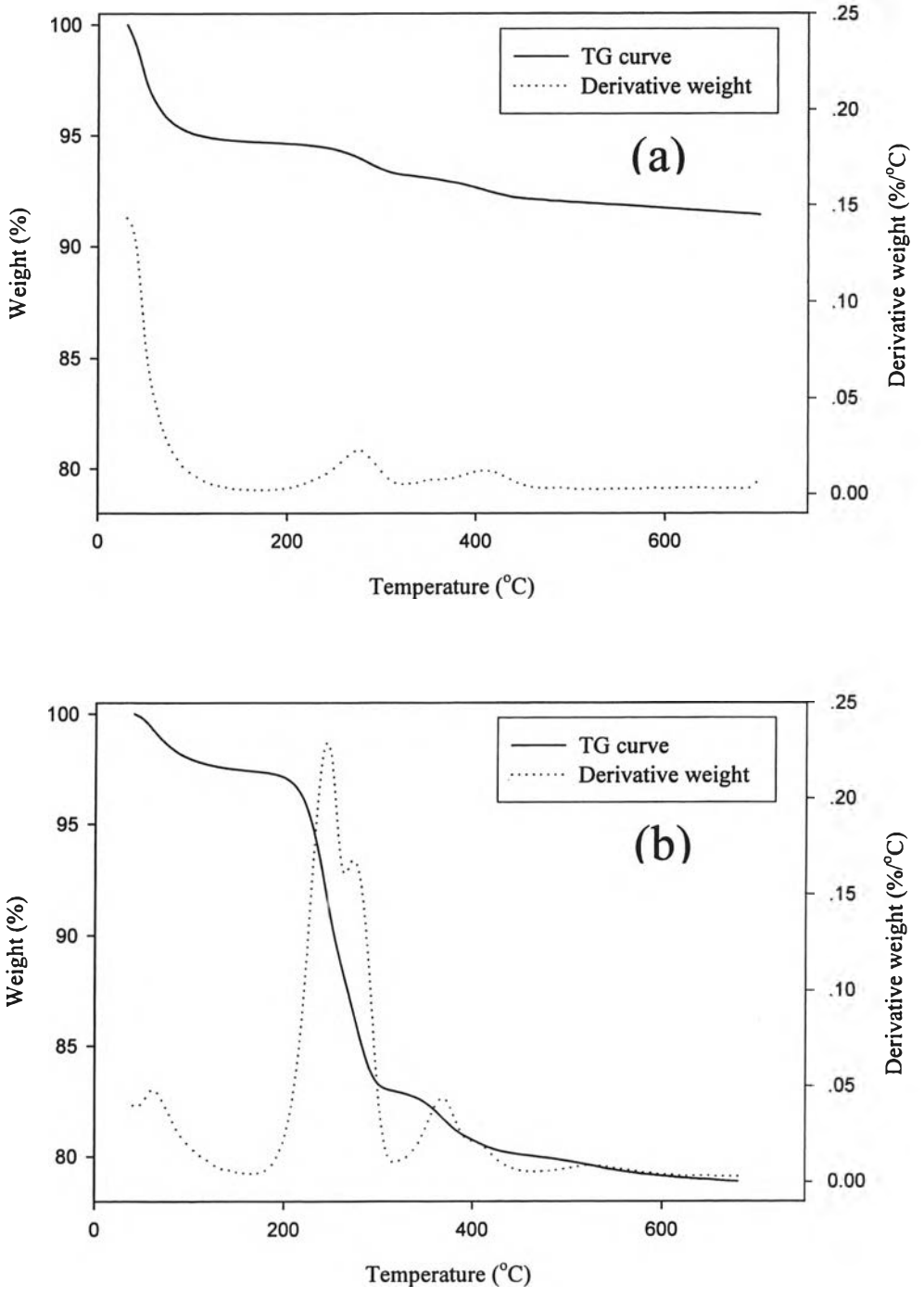

Figure 4.18 TGA traces of adsorbed CTAB on silica surface a) Rice husk silica, and b) Hi-Sil®255.

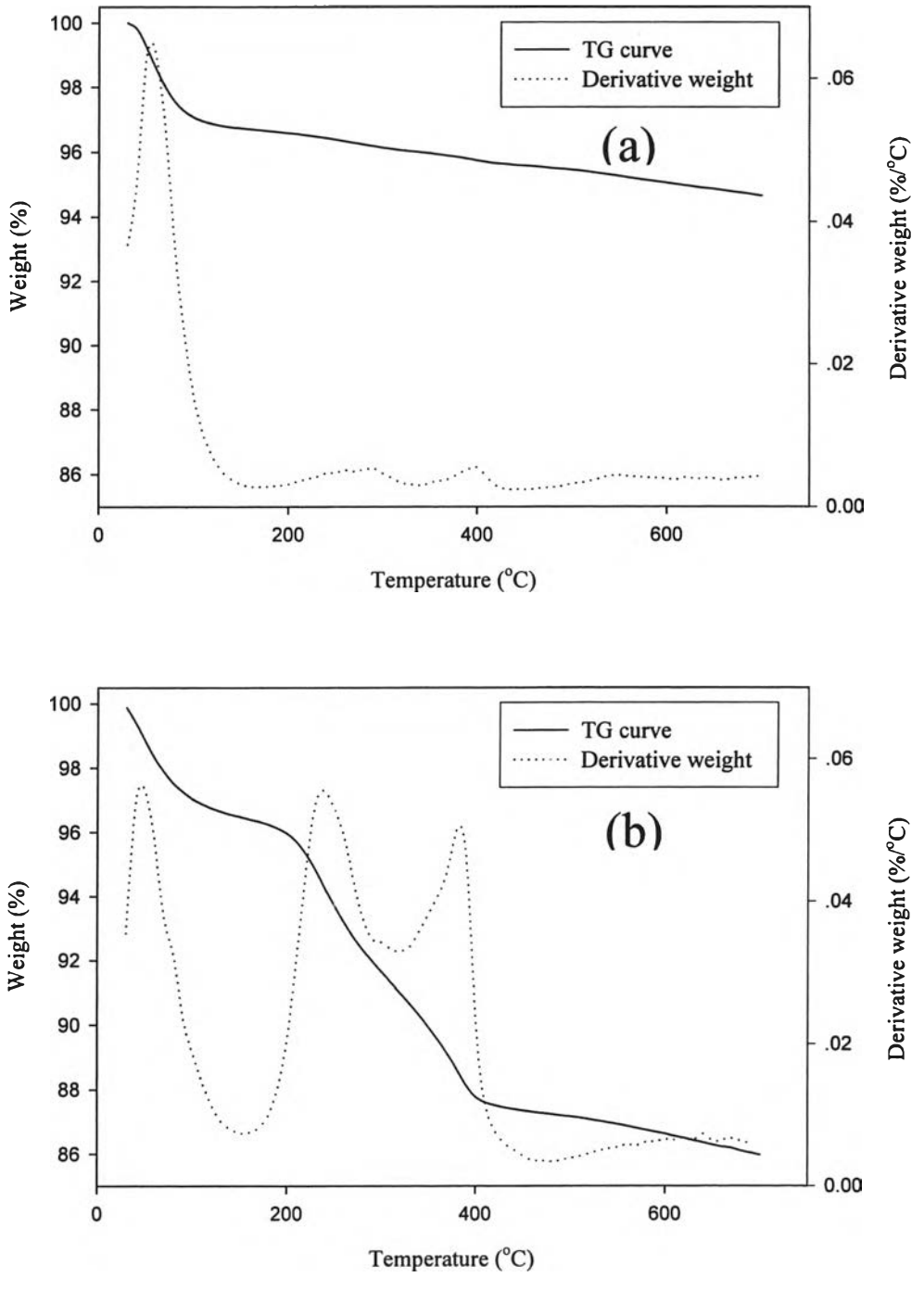

Figure 4.19 TGA traces of modified silica before extraction a) Rice husk silica, and b) Hi-Sil®255.

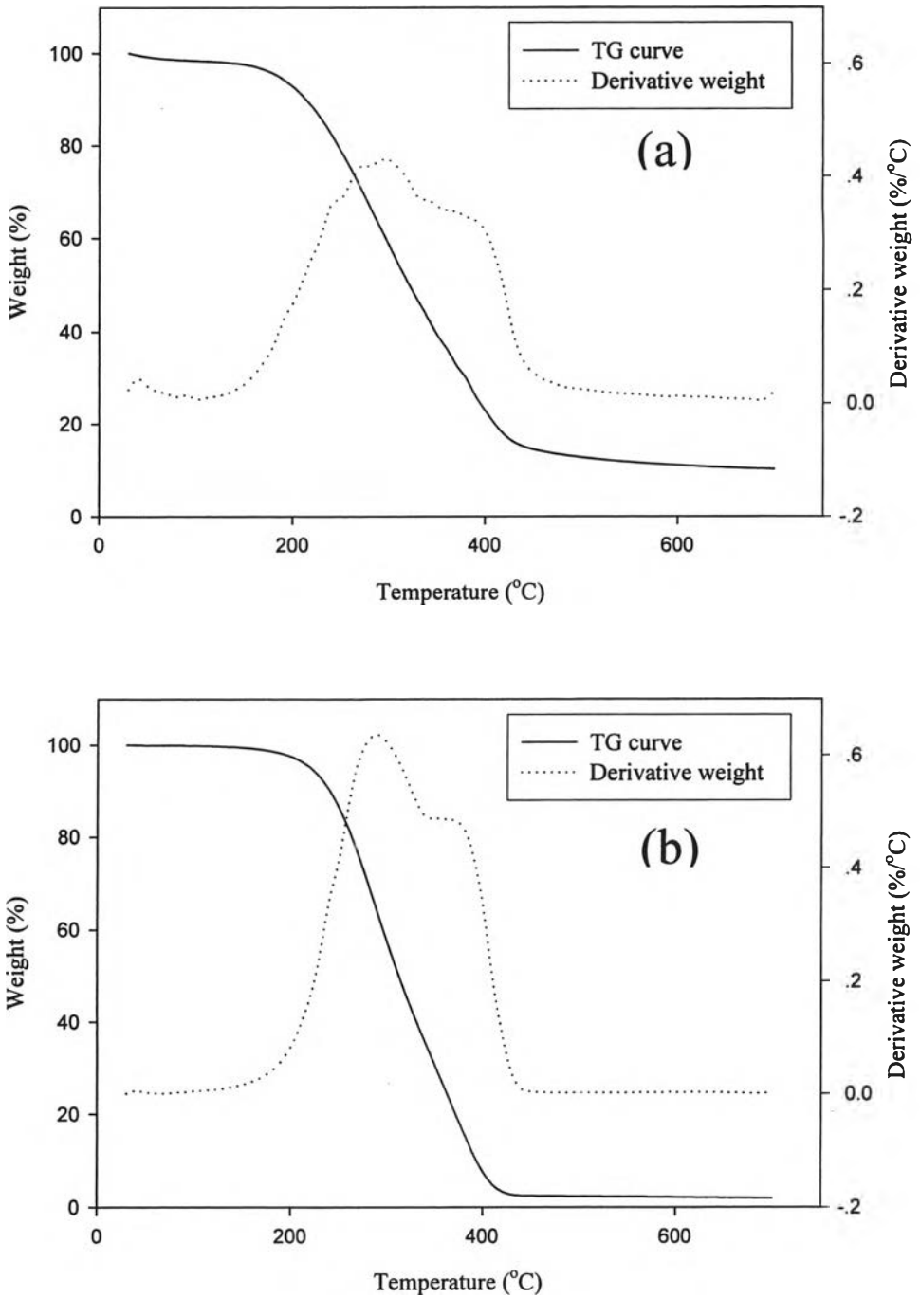

Figure 4.20 TGA traces of extracted polystyrene from modified silica a) Rice husk silica, and b) Hi-Sil®255.

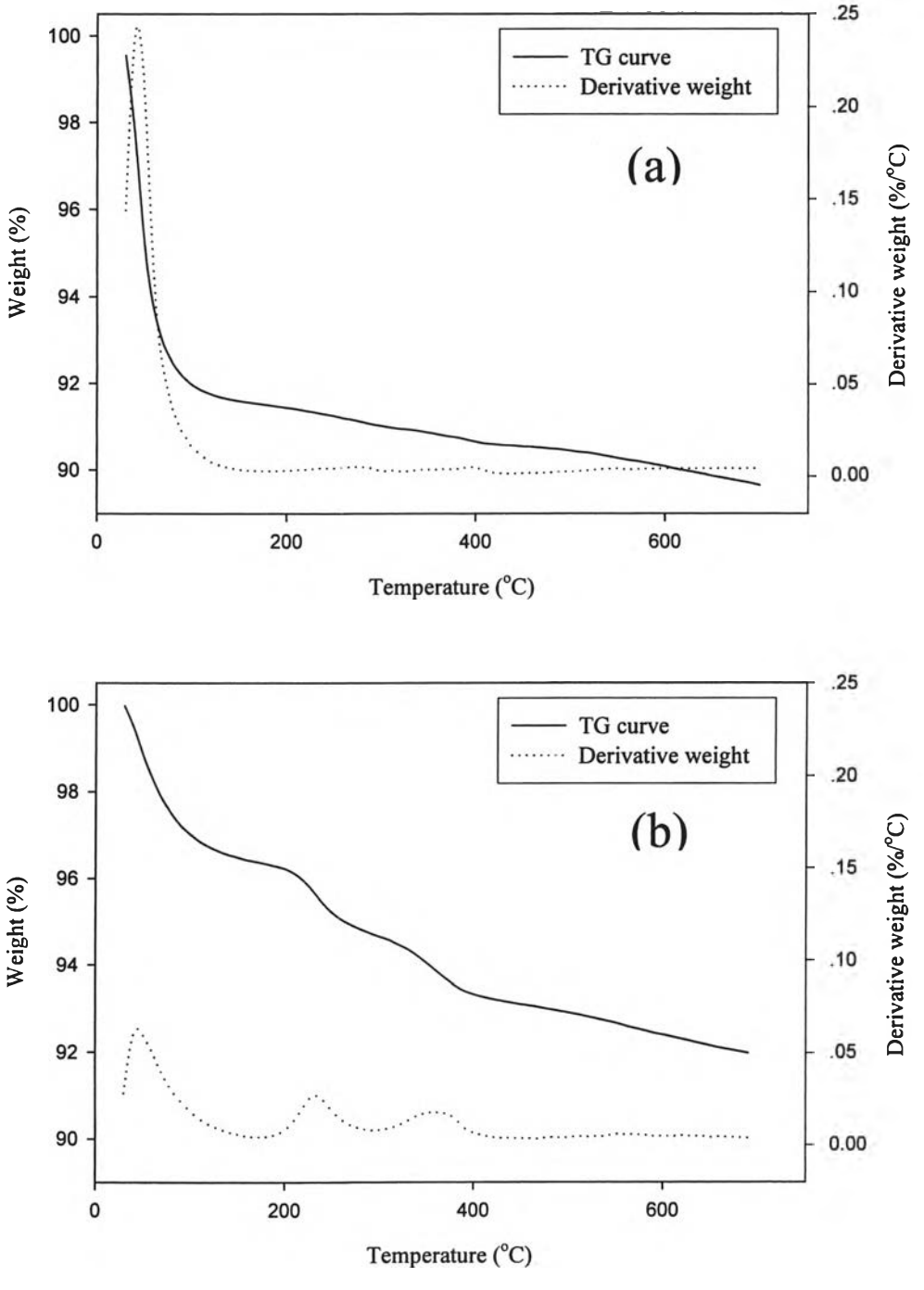

Figure 4.21 TGA traces of modified silica after extraction a) Rice husk silica, and b) Hi-Sil®255.

4.2.4 Molecular Weight Measurement

The molecular weight of the extracted polystyrene was determined using gel permeation chromatography (GPC) technique.

Table 4.3 illustrates the number average molecular weight ($\overline{M}_n$), weight average molecular weight ($\overline{M}_w$), and molecular weight distribution (MWD) of the extracted polystyrene from both modified rice husk silica and modified Hi-Sil®255.

Table 4.3 $\overline{M}_n$, $\overline{M}_w$, and MWD of extracted polystyrene from modified silica

Extracted polystyrene	$\overline{M}_n$ ($gmol^{-1}$)	$\overline{M}_w$ ($gmol^{-1}$)	MWD
Rice husk silica	685	832	1.21
Hi-Sil®255	707	885	1.25

As a result, the weight average molecular weights of the extracted polystyrene from rice husk silica and Hi-Sil®255 were not high. The GPC curves of the extracted polystyrene for both types of silica showed only one peak. The weight average molecular weights of the extracted polystyrene from rice husk silica and Hi-Sil®255 were 885 and 832 $gmol^{-1}$, respectively. These results suggested that the extracted polystyrene from both modified silicas were short chains polystyrene or growing chain polystyrene. It could also be possible that 1) incomplete removal of polystyrene from the silicas, 2) the ratio of initiator (AIBN) and monomer (styrene) used in the admicellar polymerization process was too high. Thus, the polystyrene obtained was low molecular weight polymer.

4.2.5. Morphology of Modified Silica

The scanning electron micrographs of the rice husk silica and Hi-Sil®255 with surface modification by admicellar polymerization of styrene are shown

in Figure 4.22. Comparisons between the unmodified and modified surface of both silicas also show that the surfaces of the modified silica appeared rougher than that of the unmodified silica. For the reason that the polymerization of polystyrene on the silica surface resulted in the rough appearance. Table 4.4 illustrates the BET specific surface area of the modified surface of both silicas compared with those of both unmodified silicas. As expected, the BET specific surface area of both modified silicas decreased about 18% after surface modification via admicellar polymerization process. These results suggested that the polystyrene covers or obstructs the pores of silica leading to decrease in BET specific surface area of the modified silicas. These results show a good correlation between surface roughness and a reduction in the BET specific surface area of the modified silica as shown in Figure 4.22 and Table 4.4, respectively.

Table 4.4 BET surface area, pore volume and pore size of modified silica

Sample	BET surface area (m^2/g)	Pore Volume (cc/g)	Pore Diameter (A°)
Rice husk silica	283.8	0.4878	68.74
Unmodified rice husk silica	349.4	0.4612	52.80
Hi-Sil®255	150.5	1.953	519.3
Unmodified Hi-Sil®255	184.7	1.514	328.0

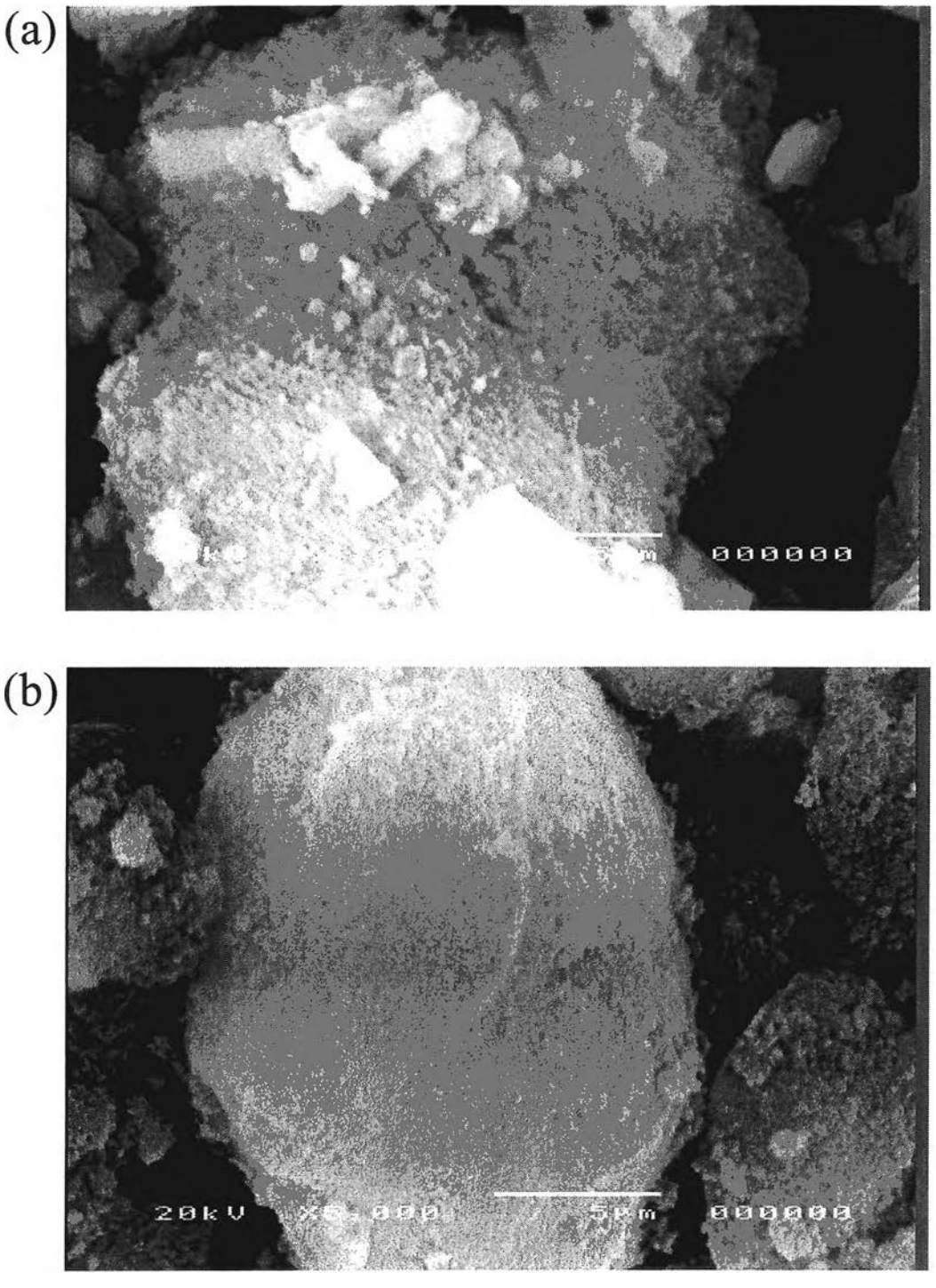

Figure 4.22 SEM micrographs of modified silica a) Rice husk silica, and b) Hi-Sil®255.